NANO LETTERS

pubs.acs.org/NanoLett Letter

High-Speed Modulation of Polarized Thermal Radiation from an On-Chip Aligned Carbon Nanotube Film

Shinichiro Matano, Natsumi Komatsu, Yui Shimura, Junichiro Kono, and Hideyuki Maki*

Cite This: *Nano Lett.* 2023, 23, 9817−9824 Read Online

ACCESS | Metrics & More | Article Recommendations | Supporting Information

ABSTRACT: Spectroscopic analysis with polarized light has been widely used to investigate molecular structure and material behavior. A broadband polarized light source that can be switched on and off at a high speed is indispensable for reading faint signals, but such a source has not been developed. Here, using aligned carbon nanotube (CNT) films, we have developed broadband thermal emitters of polarized infrared radiation with switching speeds of ≲20 MHz. We found that the switching speed depends on whether the electrical current is parallel or perpendicular to the CNT alignment direction with a significantly higher speed achieved in the parallel case. Together with detailed theoretical simulations, our experimental results demonstrate that the contact thermal conductance to the substrate and the conductance to the electrodes are important factors that determine the switching speed. These emitters can lead to advanced spectroscopic analysis techniques with polarized radiation.

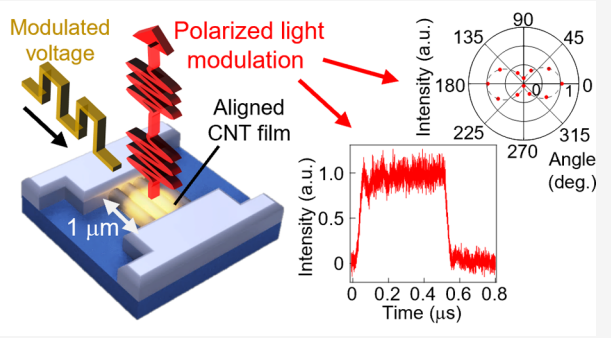

KEYWORDS: *high-speed light emitter, polarized light, thermal radiation, aligned carbon nanotube film, anisotropy*

A source for polarized broadband radiation is essential in polarized spectroscopic techniques for crystallinity analysis, stereochemical studies of organic and inorganic molecules, and biomolecule identification in physics, chemistry, and biology.[1−3] A variety of chemical and biochemical molecules and natural products have asymmetric structures, and identification of these structures is key to understanding material characteristics such as product quality checks and drug discovery. To detect even smaller signals in these spectroscopic measurements, a polarized radiation source that can be turned on and off at a high speed is desired for performing modulation spectroscopy. Conventionally, thermally activated sources such as ceramic and halogen lamps have been used, but their modulation speeds are low (∼10 Hz) because of their large heat capacities. External modulators such as mechanical choppers can be used to achieve faster modulations (<10 kHz), but the entire measurement system becomes bulky. Acousto-optic and electro-optic modulators have much higher modulation speeds (>200 MHz), but they cannot be used for broadband light.

Thermal radiation from carbon nanomaterials is promising for overcoming these challenges. Electrically driven infrared radiation sources covering a wide wavelength range have been recently developed using graphene[4,5] and carbon nanotubes (CNTs).[6,7] Thermal radiation from these materials is based on blackbody radiation,[6−17] but their response to direct electrical modulations is expected to be fast due to their small heat capacities. However, polarized and spectrally broad emission with a high modulation speed has not been reported because graphene[4,5] and randomly oriented CNTs[7] were used in previous modulation studies.

Here, we demonstrate high-speed (∼20 MHz) switching of polarized broadband infrared thermal radiation from films of aligned and densely packed CNTs. Our previous work using aligned CNT films has demonstrated electrically driven polarized thermal radiation covering a wide infrared wavelength range.[17] In the work presented here, we found that the electrical switching on/off time depends on whether the electrical current direction is parallel or perpendicular to the CNT alignment direction. When the alignment direction was parallel to the channel direction, the highest modulation speed was achieved. Our thermal transfer simulations show that the switching speed is determined not only by the contact thermal conductance to the substrate but also by the contact thermal conductance to the electrodes. Furthermore, we also demonstrated that the speed strongly depends on the film size, with smaller devices showing faster switching. These findings provide useful knowledge for developing carbon-based polarized thermal radiation sources.

Received: July 9, 2023
Revised: September 10, 2023
Published: October 26, 2023

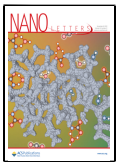

https://doi.org/10.1021/acs.nanolett.3c02555
Nano Lett. 2023, 23, 9817−9824

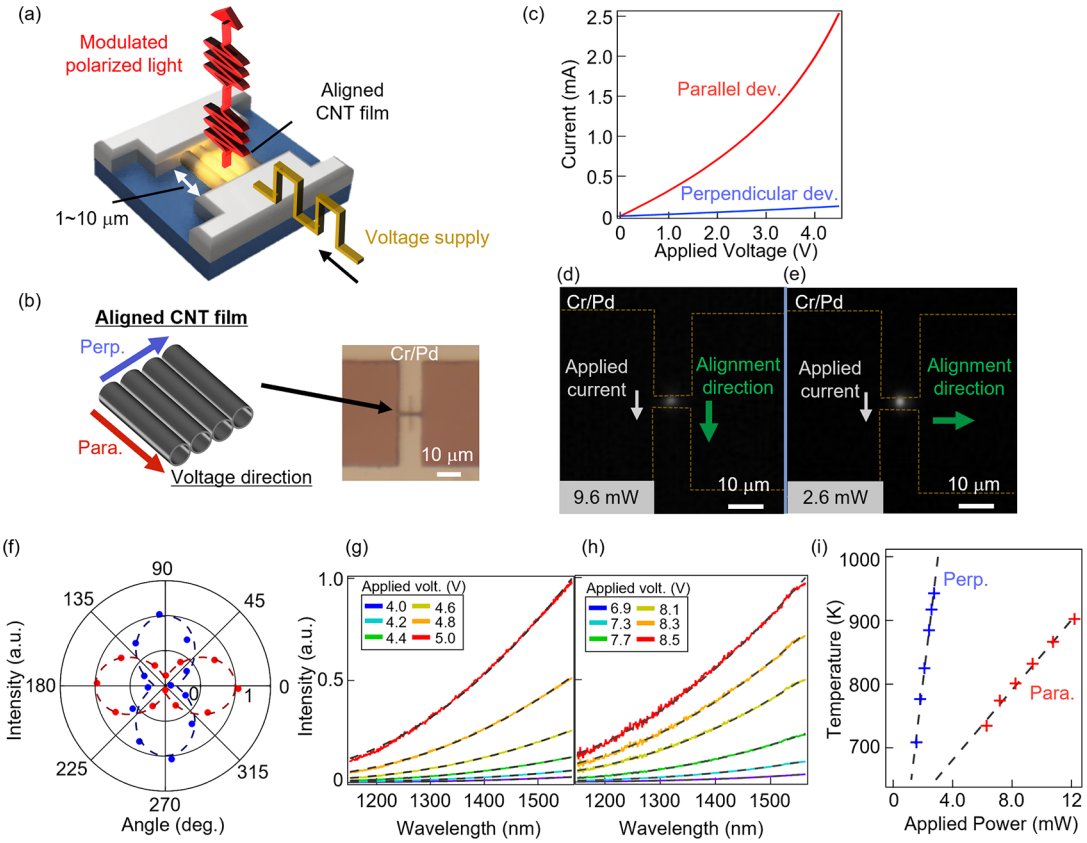

Figure 1. Structure and emission characteristics of the aligned carbon nanotube film device under a dc bias voltage. (a) Schematic diagram of an electrically driven thermal emission device based on an aligned CNT film. (b) Optical microscope image of a fabricated device and annotation for the voltage direction with respect to the CNT alignment direction. (c) Current−voltage characteristics of the parallel (red curve) and perpendicular (blue curve) devices. (d and e) Infrared radiation emission images of the parallel and perpendicular devices, respectively, with an integration time of 20 ms. The applied power is noted at the corners of the figures. (f) Polarization properties of the emitted radiation from the parallel (red) and perpendicular (blue) devices. The polarizer orientation is initialized in the current direction. These polarization results can be fit with $I_{\perp} + (I_{\parallel} - I_{\perp})\cos^2(\theta)$, where $I_{\parallel}$ and $I_{\perp}$ are the intensities of emitted radiation polarized parallel and perpendicular, respectively, to the CNT alignment direction and θ is the angle between the polarized direction and the CNT alignment direction. (g and h) Emission spectra of the parallel and perpendicular devices, respectively, at various applied voltages. Each spectrum can be fit well with the Planck formula (dashed curves). (i) Device temperatures estimated from the emission spectra for parallel (red) and perpendicular (blue) devices. The dashed lines are linear fits that can be used to estimate the device temperature from the applied power.

Figure 1a schematically shows the electrically driven CNT thermal emitter that we fabricated. We used the controlled vacuum filtration method[18,19] to prepare CNT films in which CNTs were macroscopically well aligned and densely packed.[18−24] We created two types of devices that are schematically shown in Figure 1b: a "parallel device", in which the current direction was parallel to the CNT alignment direction, and a "perpendicular device", in which the current direction was perpendicular to the CNT alignment direction. Cr/Pd electrodes were formed on a 60 nm thick CNT film on a SiO_2/Si substrate, and the exposed area of the film was 1 μm × 1 μm. Figure 1c shows the $I-V$ characteristics of the parallel and perpendicular devices, demonstrating strong anisotropy with low-bias resistances of 3.23×10^3 and 4.62×10^4 Ω, respectively.

From both devices, we observed infrared thermal emission under bias. Panels d and e of Figure 1 show emission images of the parallel and perpendicular devices, respectively, taken with an infrared camera. Note that both images were obtained with the same integration time (20 ms), but the applied powers were different (9.6 mW vs 2.6 mW). This result indicates different amounts of heat transfer to the electrodes between the two devices because the rate of dissipation of heat to the substrate can be assumed to be the same. In the perpendicular device, thermal dissipation to the electrodes is expected to be suppressed, compared to that of the parallel device, because of the lower thermal conductivity along the current direction. In addition, we observed that the emitted radiation was linearly polarized in both devices and that the polarization direction was parallel to the CNT alignment direction independent of the applied current direction (see Figure 1f). This behavior reflects the strong optical anisotropy of our aligned CNT film. Previous studies have reported strongly anisotropic permittivities for aligned CNT films, including hyperbolic behaviors in a wide infrared spectral range.[22,25] The polarized emission from our devices can thus be understood in terms of anisotropic emissivity through Kirchhoff's law.

Panels g and h of Figure 1 show emission spectra in the near-infrared range for parallel and perpendicular devices, respectively. We observed broadband thermal emission, whose spectra could be fit by Planck's law (dashed curves). Figure 1i shows the temperature obtained from the fits as a function of the applied power. In both devices, the temperature increases linearly with the applied power in the infrared observable

https://doi.org/10.1021/acs.nanolett.3c02555
Nano Lett. 2023, 23, 9817−9824

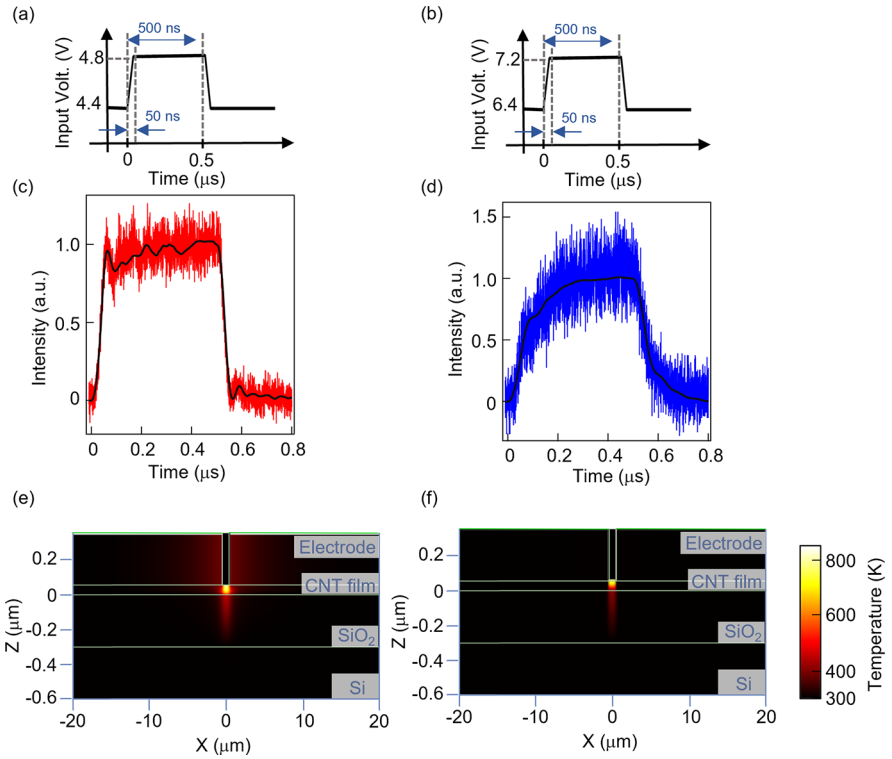

Figure 2. Time-resolved emission intensities in the parallel and perpendicular devices. Time-resolved thermal emission under a rectangular voltage in the (a) parallel (4.4−4.8 V) and (b) perpendicular (6.4−7.2 V) devices. (c) Time-resolved intensities of emitted radiation from the parallel device, measured experimentally (red curve) and simulated (black curve). (d) Time-resolved intensities of emitted radiation from the perpendicular device measured experimentally (blue curve) and simulated (black curve). Calculated temperature distributions when the emission intensity is the maximum (t = 500 ns) for the (e) parallel and (f) perpendicular devices. For the two-dimensional thermal simulation, we chose the cross-sectional face of a device. Both simulation results are illustrated with different scales on the vertical and horizontal axes for the sake of clarity.

region. This linear relation can be explained by a one-dimensional thermal transfer model, as discussed in ref 17. In the work presented here, we used this linear relation between the device temperature and the applied power for the simulations presented below. From this relation between applied power and estimated temperature, we estimated the thermal radiation efficiency of the parallel (perpendicular) device at T = 800 K to be ~2.8×10^{-6} (~1.2×10^{-5}) (see the Supporting Information for the calculation details).

To investigate the modulation/switching speeds that can be achieved with these aligned CNT emitters, we performed time-resolved measurements of the emission intensity in the parallel (Figure 2c) and perpendicular (Figure 2d) devices in response to a rectangular voltage input pulse depicted in panels a and b, respectively, of Figure 2. The voltage increased from a low level to a high level within 50 ns, stayed at a high level for 450 ns, and returned to the low level within 50 ns. The two devices exhibited distinctly different behaviors. In the parallel device, the thermal emission intensity quickly increased at almost the same speed as the voltage increase and then saturated at the high level of the voltage. In the perpendicular device, the light emission intensity increased more slowly and did not saturate at the high level of the voltage. Also, in the falling part, the intensity decrease in the parallel device was faster than that in the perpendicular device.

To understand the mechanism of these differences in switching speeds between the parallel and perpendicular devices, we performed numerical simulations of time-dependent emission intensities; the results are shown as black curves in panels c and d of Figure 2. The simulations were based on a thermal transfer model that included transfer both to the electrodes and to the substrate (see the Supporting Information for more details of the model). Our simulation results and the experimental results demonstrate excellent agreement, explaining the observed anisotropic switching times in terms of thermal transfer along the CNT alignment direction. The switching speed can be evaluated through a relaxation time (τ), which can be approximately given by the equation $\tau = C/G_{tot}$, where C is the heat capacity of CNTs and G_{tot} is the sum of the thermal conductances to the electrodes and substrate.[5,7] Through the simulations, we estimated τ to be 21 ns (69 ns) for the parallel (perpendicular) device. The parallel device has a higher thermal conductivity along the current direction,[24] which leads to greater thermal transfer to the electrodes and thus a larger G_{tot}, i.e., smaller τ. On the contrary, we found that thermal transfer to the electrodes can be ignored in the perpendicular device; G_{tot} can be treated as the thermal conductance to the substrate alone, leading to a larger τ. Calculated temperature distributions (Figure 2e,f) show that the electrode temperature increases under bias only in the parallel device, which confirms that thermal transfer to the electrodes is important only in the parallel device.

To gain further insights into the time-dependent emission properties of the devices, we performed simulations as a function of junction thermal conductances: the CNT−substrate junction conductance per unit area, g_{sub}, and the CNT−electrode junction conductance per unit area, g_{elec}, as summarized in Figure 3. In the parallel device, the calculated results show two components of relaxation, especially when $g_{elec} > 1.0 \times 10^7$ W m^{-2} K^{-1}: an initial fast response and a

https://doi.org/10.1021/acs.nanolett.3c02555
Nano Lett. 2023, 23, 9817−9824

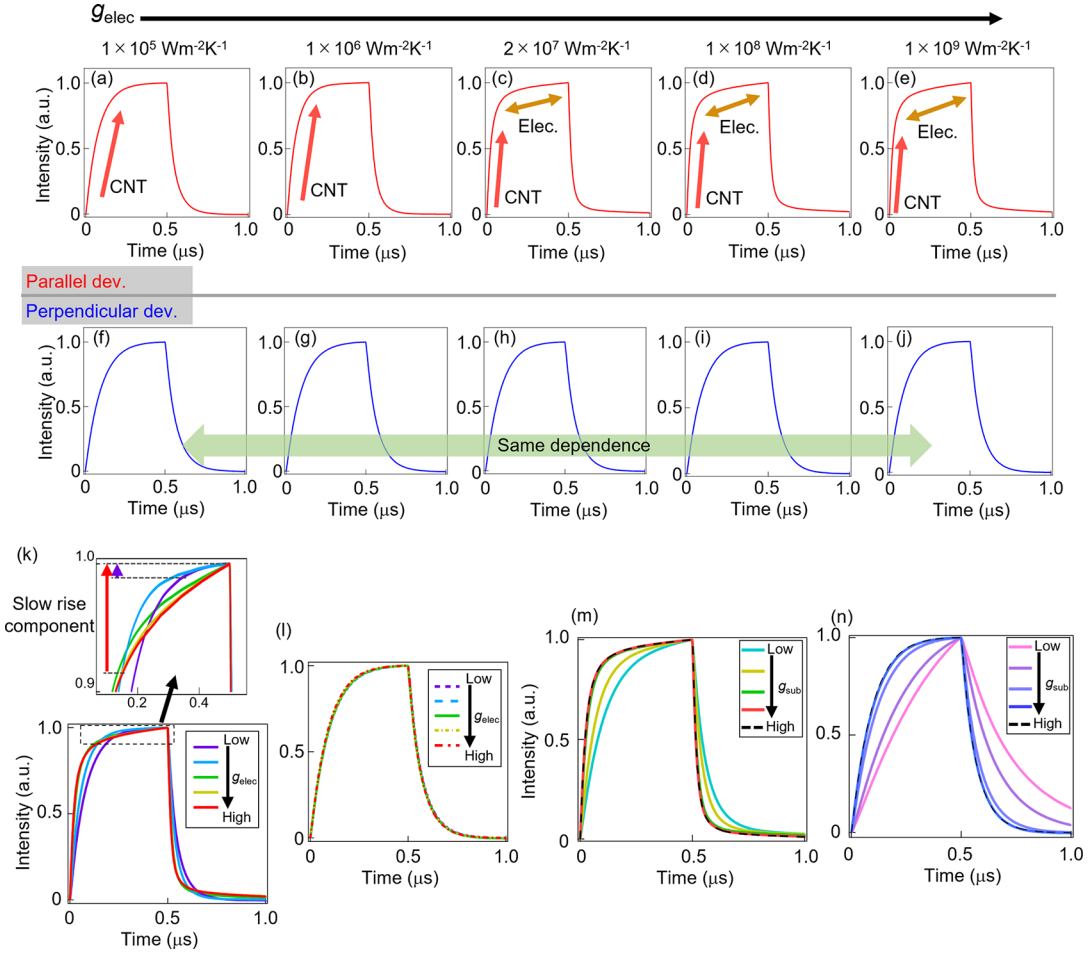

Figure 3. Calculated time-resolved thermal emission intensities for different values of g_{elec} and g_{sub}. Time-resolved emission intensities calculated on the thermal transfer simulation while changing the value of g_{elec} for the (a–e) parallel and (f–j) perpendicular devices. The input was an ideal rectangular voltage with a width of 500 ns in the (a) parallel (4.4–4.8 V) and (b) perpendicular (6.4–7.2 V) devices. In the simulation, values of 1×10^5 W m^{-2} K^{-1} (a and f), 1×10^6 W m^{-2} K^{-1} (b and g), 2×10^7 W m^{-2} K^{-1} (c and h), 1×10^8 W m^{-2} K^{-1} (d and i), and 1×10^9 W m^{-2} K^{-1} (e and j) were used for g_{elec}, and the value of 2×10^7 W m^{-2} K^{-1} is a reference value from the previous report.[37] (k and l) Time-resolved emission intensities for the parallel and perpendicular devices, respectively, in overlapped graphs. Purple, blue, green, yellow, and red curves correspond to the intensities under the condition that the values of g_{elec} are 1×10^5, 1×10^6, 2×10^7, 1×10^8, and 1×10^9 W m^{-2} K^{-1}, respectively. The top graph in panel k focuses on the second increase in the emission intensities. (m and n) Time-resolved emission intensities calculated while changing the value of g_{sub} for the parallel and perpendicular devices, respectively. For the parallel device, values of 1×10^5 W m^{-2} K^{-1} (blue), 1×10^6 W m^{-2} K^{-1} (yellow), 1×10^7 W m^{-2} K^{-1} (green), 5×10^7 W m^{-2} K^{-1} (red), and 1×10^9 W m^{-2} K^{-1} (dashed black) were used for g_{sub}, and on the perpendicular device, values of 1×10^6 W m^{-2} K^{-1} (pink), 2×10^6 W m^{-2} K^{-1} (purple), 1×10^7 W m^{-2} K^{-1} (light blue), 5×10^7 W m^{-2} K^{-1} (blue), and 1×10^9 W m^{-2} K^{-1} (dashed black) were used for g_{sub}. For both devices, the value of 5×10^7 W m^{-2} K^{-1} is a reference value from the previous report.[32]

subsequent slower response. As g_{elec} increases, the first component becomes faster while, at the same time, the second component becomes larger (emphasized in the inset of Figure 3k). The initial emission response with a fast increase indicates a temperature increase in the CNT film itself. The initial response speed increases with g_{elec} because the total thermal dissipation rate increases. The second component with a slower increasing rate is caused by the temperature increase of the electrodes. The heat capacity of the electrode metal is larger than that of CNTs, and thus, the electrode temperature increase is slower. In the perpendicular device, there is no dependence on g_{elec} (Figure 3l), indicating that thermal dissipation predominantly occurs through transfer to the substrate. Panels m and n of Figure 3 show calculated time-dependent emission intensities in the parallel and perpendicular devices, respectively, for different values of g_{sub}. The switching speed increases with g_{sub} in both devices, which is expected and is consistent with the results reported in previous studies.[5]

Figure 4a shows the calculated relaxation time of the CNT thermal emission intensity as a function of g_{elec}. The relaxation time was estimated through an exponential fit with the falling part in Figure 3a–j (see the Supporting Information for more details). As shown in Figure 4a, the relaxation time decreases with an increase in g_{elec} in the parallel device, while it is essentially constant in the perpendicular device. This result indicates that the larger g_{elec} in the parallel device creates a difference in relaxation time between the two devices. The thermal dissipation rate depends on the thermal resistances shown inside the red squares of panels c and d of Figure 4. In the parallel device, the thermal resistance in the channel direction (R_{ch}) is small due to the large thermal conductivity in the CNT alignment direction, and thus, the total resistance is the thermal resistance to the electrode plus that to the

https://doi.org/10.1021/acs.nanolett.3c02555
Nano Lett. 2023, 23, 9817–9824

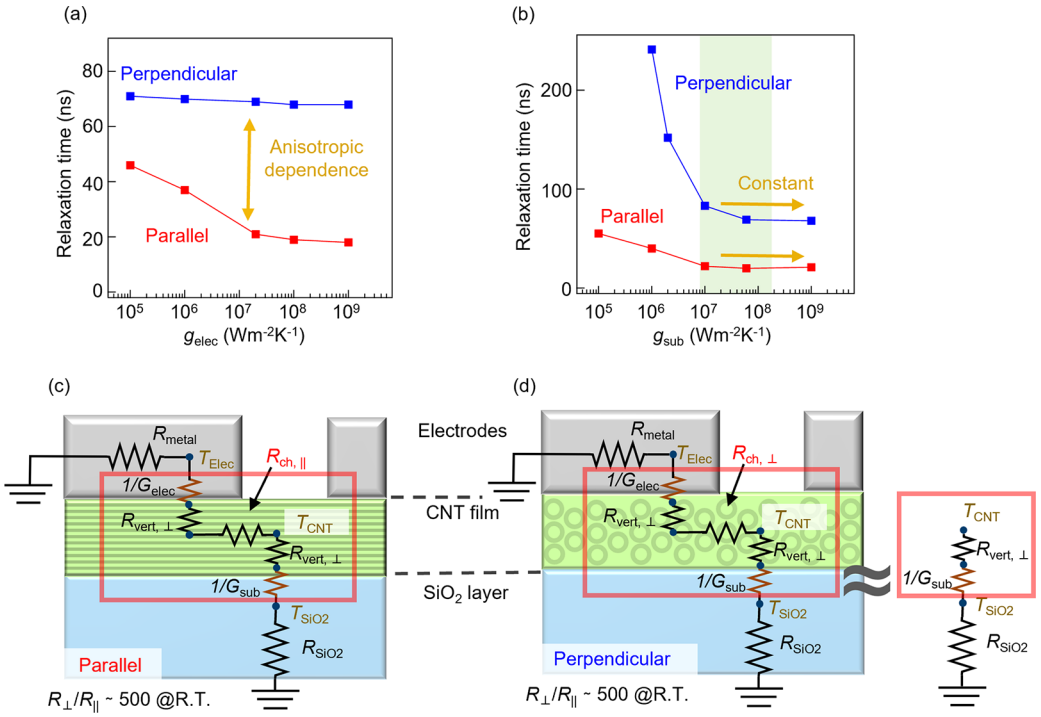

Figure 4. Relaxation time of emission calculated for the parallel and perpendicular devices for different values of g_{elec} and g_{sub}. Calculated relaxation time of emission derived from the CNT temperature increase vs (a) g_{elec} and (b) g_{sub} for the parallel (red) and perpendicular (blue) devices. The relaxation time was estimated by using a relaxation function to fit the falling part of the emission intensity. The green range of panel b (8×10^6 to 2×10^8 W m^{-2} K^{-1}) shows the typical value of contact thermal conductance between the carbon nanomaterial (CNTs or graphene) and substrate reported in the previous studies.[26,32,35] (c and d) Equivalent thermal transfer circuits representing the parallel and perpendicular devices, respectively.

substrate. In the perpendicular device, because R_{ch} is large, the thermal resistance is only the resistance to the substrate. This system difference results in a difference in the relaxation time (Figure 4a). The effects of contact between an electrode and CNTs are usually small and have been neglected or difficultly discussed in previous studies.[11,24,26−34] In the work presented here, the anisotropic properties of the aligned CNT films enabled us to identify such small effects of thermal contact with the electrodes clearly.

Figure 4b shows the g_{sub} dependence of the relaxation time, estimated from panels m and n of Figure 3 (see the Supporting Information). In both devices, the relaxation time decreases with an increase in g_{sub} in the low-g_{sub} region and is almost constant in the high-g_{sub} region. The constant relaxation time in the high-g_{sub} region is due to the relatively high CNT resistance (i.e., R_{vert} and R_{ch} in panels c and d of Figure 4). This result shows that the response characteristic is stable in the typical g_{sub} range from 8×10^6 to 2×10^8 W m^{-2} K^{-1} (indicated by the green region in Figure 4b), as previously reported.[26,32,35] Because the contact thermal conductance is sensitive to the physical contact condition between the the CNT and substrate, the stable behavior of the relaxation time in the typical g_{sub} range can contribute to stable fabrication of a thermal light emitter using carbon nanomaterials.

Finally, to study how the emitter size affects the switching speed, we fabricated additional parallel square devices, which had lateral sizes of 2 μm × 2 μm, 7 μm × 7 μm, and 10 μm × 10 μm. Panels a (experiment) and b (simulation) of Figure 5 show time-resolved light emission intensities for these four devices, indicating that a smaller device has a higher switching speed. The simulation investigation suggests that a shorter channel length especially contributes to the faster response of the emitter due to the higher rate of dissipation of heat to the electrodes. Panels c and d of Figure 5 show calculated temperature distributions for the 1 and 10 μm devices, respectively. In the 10 μm device, thermal transfer to the electrodes is suppressed and heat mainly dissipates to the substrate (Figure 5c), while in the 1 μm device, heat can efficiently dissipate to the electrodes in addition to the substrate (Figure 5d). This can be confirmed by the steeper slope of the CNT temperature distribution and the greater electrode heating in the 1 μm device than in the 10 μm device (highlighted in the top graphs in panels c and d of Figure 5). Hence, the small fabrication (1 μm × 1 μm) enables us to produce higher switching thermal emitters.

We achieved high-speed switching of polarized thermal radiation by using aligned CNT films with a relaxation time of ~20 ns. The speed is strongly enhanced when the CNT alignment direction is parallel to the current direction. Two-dimensional thermal transfer simulations revealed that the electrode contacts play an important role in the current direction dependence of the speed. The switching speed is stable in the typical range of the contact thermal conductance to the substrate, which allows for a stable quality of fabricated high-speed emitters. In further device size-dependent investigations, we demonstrated that smaller devices (e.g., 1 μm × 1 μm) have higher speeds. This emitter enables high-speed modulations of polarized and broadband radiation from a microscale structure on a silicon chip. This aligned CNT-based compact emitter can be rapidly turned on and off, in contrast to bulky and slow incandescent light sources. This high-speed property can greatly improve the sensitivity of polarized

https://doi.org/10.1021/acs.nanolett.3c02555
Nano Lett. 2023, 23, 9817−9824

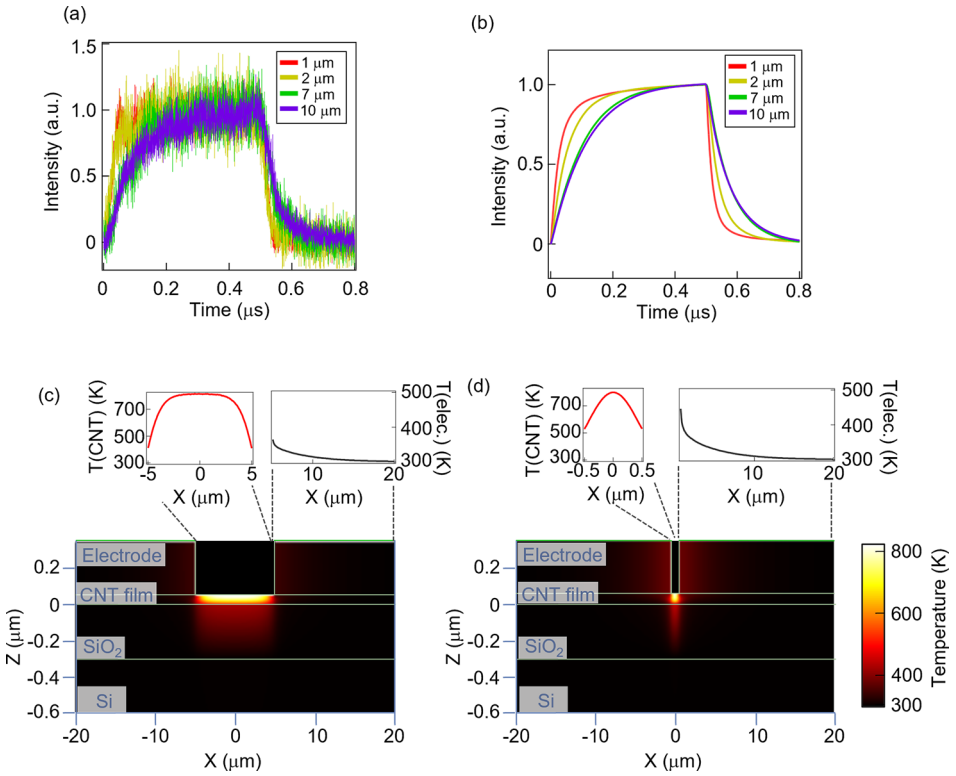

Figure 5. Response speed as a function of device size. Time-resolved emission intensities in parallel devices were (a) measured experimentally and (b) simulated under a rectangular voltage with a width of 500 ns. The applied voltages were changed to obtain the same emission intensity in the devices. Detailed information about the applied voltages is described in Experiential Methods. The red, yellow, green, and purple curves correspond to data for devices with lateral sizes of 1 μm × 1 μm, 2 μm × 2 μm, 7 μm × 7 μm, and 10 μm × 10 μm, respectively. The lateral lengths of the square devices are written in the legend. In the simulation, an ideal rectangular voltage was used as the input. Calculated temperature distributions when the intensities are maximum (t = 500 ns) for the (c) 10 and (d) 1 μm devices. The top left (right) graphs exhibit a CNT (electrode) temperature distribution in the vicinity of Z = 60 nm (the boundary between the electrodes and the CNT film). Both simulation results are illustrated with different scales on the vertical and horizontal axes for the sake of clarity.

spectroscopic systems by using synchronous signal detection techniques.[36]

EXPERIMENTAL METHODS

Device Fabrication. In this work, we fabricated thermal light emitters based on a macroscopically aligned CNT film. CNT films were prepared by the controlled vacuum filtration method.[18] We used commercially available SWCNTs (P2-SWNT) produced by the arc-discharge method from Carbon Solution, Inc. The average diameter of the SWCNTs was 1.4 nm, and the sample contained both metallic and semiconducting SWCNTs (see ref 18 for detailed information about the film's preparation). In brief, SWCNTs were suspended in water with 0.01% (w/v) sodium deoxycholate (Sigma-Aldrich) and filtered with polycarbonate filter membranes at slow filtration speeds of approximately 1−2 mL/h. We used 60 nm thick CNT films and placed them onto a silicon substrate with a 300 nm silicon oxide layer by using the wet transfer method.[38] To fabricate light-emitting devices on a silicon substrate, an aligned CNT film was shaped through photolithography and O_2 plasma etching and covered with Cr/Pd electrodes with a gap for each channel length. In this research, we prepared light-emitting devices with exposure areas of 1 μm × 1 μm, 2 μm × 2 μm, 7 μm × 7 μm, and 10 μm × 10 μm. By controlling the channel direction against the CNT alignment direction, we fabricated parallel and perpendicular devices where the channel direction is along and perpendicular to the alignment axis, respectively.

Infrared Optical Measurement for a Microsized Thermal Light Emitter. We measured thermal emissions under a bias voltage and time-resolved thermal emission to understand the basic emission characteristics. In a micro photoluminescence measurement system,[5,7,17,39] a light-emitting device was set in a vacuum chamber with a quartz optical window, and the bias voltage and square wave voltage were applied to a device inside the chamber with a dc voltage source and a function generator, respectively. To achieve the same light intensity in parallel and perpendicular devices, we applied a rectangular voltage with 4.4 and 6.4 V for low voltages and 4.8 and 7.2 V for high voltages, respectively. For 1, 2, 7, and 10 μm square parallel devices, we applied a rectangular voltage with 4.4, 3.4, 4.0, and 4.2 V for low voltages and 4.8, 3.7, 4.5, and 4.7 V for high voltages, respectively. The applied voltages were changed to obtain the same emission intensity in these devices. The shape of the input voltages is similar to the shape in the 1 μm square parallel device. Through a microscope objective lens, the emitted light was observed and guided to either an InGaAs CCD camera or an InGaAs linear array detector with a spectrometer to obtain two-dimensional (2D) light emission images or emission spectra, respectively. The detectable wavelength range of the CCD camera and the linear array detector was 900−1600 nm. The polarization properties were measured by combining a polarizer with an infrared camera. To obtain the relative spectral response of the optical

https://doi.org/10.1021/acs.nanolett.3c02555
Nano Lett. 2023, 23, 9817−9824

measurement system, including the optical path and the detector, standard light was used, which was generated from a blackbody furnace. In the measurement system, the emitted light was also guided to a Geiger-mode InGaAs avalanche photodiode (APD) through a fiber coupler and a multimode optical fiber to obtain the time-resolved light intensity. The detectable wavelength range was 900−1700 nm. Geiger-mode APD produces an electrical pulse when a single photon is detected, and the time-resolved light intensity is calculated by combining the detector with a time-correlated single-photon counting module (see the Supporting Information for details). Measuring the time-resolved light intensity through the single-photon counting method is effective because light can be detected accurately, regardless of the light intensity.

■ ASSOCIATED CONTENT

Supporting Information

The Supporting Information is available free of charge at https://pubs.acs.org/doi/10.1021/acs.nanolett.3c02555.

Details of the time-resolved optical measurement system, a basic calculation method for the transient thermal 2D distribution in a CNT device, description of temperature-dependent physical values, a method for estimating the relaxation time of emission intensity, and discussion of the thermal radiation power and efficiency of the devices (PDF)

■ AUTHOR INFORMATION

Corresponding Author

Hideyuki Maki − *Department of Applied Physics and Physico-Informatics, Keio University, Yokohama 223-8522, Japan; Center for Spintronics Research Network, Keio University, Yokohama, Kanagawa 223-8522, Japan;* orcid.org/0000-0001-5545-5932; Email: maki@appi.keio.ac.jp

Authors

Shinichiro Matano − *Department of Applied Physics and Physico-Informatics, Keio University, Yokohama 223-8522, Japan;* orcid.org/0000-0001-5001-3203

Natsumi Komatsu − *Department of Electrical and Computer Engineering, Rice University, Houston, Texas 77005, United States;* orcid.org/0000-0003-0959-7088

Yui Shimura − *Department of Applied Physics and Physico-Informatics, Keio University, Yokohama 223-8522, Japan*

Junichiro Kono − *Department of Electrical and Computer Engineering, Rice University, Houston, Texas 77005, United States; Department of Physics and Astronomy and Department of Materials Science and NanoEngineering, Rice University, Houston, Texas 77005, United States;* orcid.org/0000-0002-4195-0577

Complete contact information is available at: https://pubs.acs.org/10.1021/acs.nanolett.3c02555

Notes

The authors declare no competing financial interest.

■ ACKNOWLEDGMENTS

This work was partially financially supported by A-STEP (Grants JPMJTR20R4 and JPMJTR221B) and the JST-Mirai Program (Grant JPMJMI22G6) from JST and by KAKENHI (Grant 20H02210) and Partnerships for International Research and Education (PIRE, Grant JPJSJRP20221202) from JSPS. This work was technically supported by Spintronics Research Network of Japan, the Core-to-Core program from JSPS, and the NIMS Nanofabrication Platform in Nanotechnology Platform Project by MEXT. S.M. and Y.S. acknowledge support from JST SPRING (Grant JPMJSP2123), JSPS KAKENHI (Grants JP23KJ1913 and JP23KJ1903), and the Keio University Doctorate Student Grant-in-Aid Program from Ushioda Memorial Fund. N.K. and J.K. acknowledge support from the Robert A. Welch Foundation through Grant C-1509, the U.S. Air Force Office of Scientific Research through Grant FA9550-22-1-0382, the JST CREST program, Japan, through Grant JPMJCR17I5, the U.S. National Science Foundation through Grant PIRE-2230727, and the Carbon Hub of Rice University.

■ REFERENCES

(1) Sanderson, J. B. *Understanding light microscopy*; Wiley: Hoboken, NJ, 2019; pp 347−381.

(2) Berova, N.; Polavarapu, P. L.; Nakanishi, K.; Woody, R. W. *Comprehensive Chiroptical Spectroscopy, Instrumentation, Methodologies, and Theoretical Simulations*, 1st ed.; Wiley: Hoboken, NJ, 2011; pp 91−146.

(3) Berova, N. *Applications in stereochemical analysis of synthetic compounds, natural products, and biomolecules*, 1st ed.; Wiley: Hoboken, NJ, 2012; pp 3−36.

(4) Kim, Y. D.; Gao, Y.; Shiue, R. J.; Wang, L.; Aslan, O. B.; Bae, M. H.; Kim, H.; Seo, D.; Choi, H. J.; Kim, S. H.; Nemilentsau, A.; Low, T.; Tan, C.; Efetov, D. K.; Taniguchi, T.; Watanabe, K.; Shepard, K. L.; Heinz, T. F.; Englund, D.; Hone, J. Ultrafast Graphene Light Emitters. *Nano Lett.* **2018**, *18* (2), 934−940.

(5) Miyoshi, Y.; Fukazawa, Y.; Amasaka, Y.; Reckmann, R.; Yokoi, T.; Ishida, K.; Kawahara, K.; Ago, H.; Maki, H. High-Speed and on-Chip Graphene Blackbody Emitters for Optical Communications by Remote Heat Transfer. *Nat. Commun.* **2018**, *9*, 1279.

(6) Liu, P.; Liu, L.; Wei, Y.; Liu, K.; Chen, Z.; Jiang, K.; Li, Q.; Fan, S. Fast High-Temperature Response of Carbon Nanotube Film and Its Application as an Incandescent Display. *Adv. Mater.* **2009**, *21* (35), 3563−3566.

(7) Mori, T.; Yamauchi, Y.; Honda, S.; Maki, H. An Electrically Driven, Ultrahigh-Speed, on-Chip Light Emitter Based on Carbon Nanotubes. *Nano Lett.* **2014**, *14* (6), 3277−3283.

(8) Wei, J.; Zhu, H.; Wu, D.; Wei, B. Carbon Nanotube Filaments in Household Light Bulbs. *Appl. Phys. Lett.* **2004**, *84* (24), 4869−4871.

(9) Li, P.; Jiang, K.; Liu, M.; Li, Q.; Fan, S.; Sun, J. Polarized Incandescent Light Emission from Carbon Nanotubes. *Appl. Phys. Lett.* **2003**, *82* (11), 1763−1765.

(10) Aliev, A. E.; Kuznetsov, A. A. The Origin of Polarized Blackbody Radiation from Resistively Heated Multiwalled Carbon Nanotubes. *Phys. Lett. Sect. A Gen. At. Solid State Phys.* **2008**, *372* (29), 4938−4942.

(11) Estrada, D.; Pop, E. Imaging Dissipation and Hot Spots in Carbon Nanotube Network Transistors. *Appl. Phys. Lett.* **2011**, *98*, No. 073192.

(12) Fan, Y.; Singer, S. B.; Bergstrom, R.; Regan, B. C. Probing Planck's Law with Incandescent Light Emission from a Single Carbon Nanotube. *Phys. Rev. Lett.* **2009**, *102*, No. 187402.

(13) Singer, S. B.; Mecklenburg, M.; White, E. R.; Regan, B. C. Polarized Light Emission from Individual Incandescent Carbon Nanotubes. *Phys. Rev. B - Condens. Matter Mater. Phys.* **2011**, *83* (23), No. 233404.

(14) Liu, Z.; Bushmaker, A.; Aykol, M.; Cronin, S. B. Thermal Emission Spectra from Individual Suspended Carbon Nanotubes. *ACS Nano* **2011**, *5* (6), 4634−4640.

(15) Nishihara, T.; Takakura, A.; Miyauchi, Y.; Itami, K. Ultra-Narrow-Band near-Infrared Thermal Exciton Radiation in Intrinsic One-Dimensional Semiconductors. *Nat. Commun.* **2018**, *9*, 3144.

(16) Mann, D.; Kato, Y. K.; Kinkhabwala, A.; Pop, E.; Cao, J.; Wang, X.; Zhang, L.; Wang, Q.; Guo, J.; Dai, H. Electrically Driven Thermal Light Emission from Individual Single-Walled Carbon Nanotubes. *Nat. Nanotechnol.* **2007**, *2* (1), 33−38.
(17) Matano, S.; Takahashi, H.; Komatsu, N.; Shimura, Y.; Nakagawa, K.; Kono, J.; Maki, H. Electrical Generation of Polarized Broadband Radiation from an On-Chip Aligned Carbon Nanotube Film. *ACS Mater. Lett.* **2022**, *4* (4), 626−633.
(18) He, X.; Gao, W.; Xie, L.; Li, B.; Zhang, Q.; Lei, S.; Robinson, J. M.; Hároz, E. H.; Doorn, S. K.; Wang, W.; Vajtai, R.; Ajayan, P. M.; Adams, W. W.; Hauge, R. H.; Kono, J. Wafer-Scale Monodomain Films of Spontaneously Aligned Single-Walled Carbon Nanotubes. *Nat. Nanotechnol.* **2016**, *11* (7), 633−638.
(19) Komatsu, N.; Nakamura, M.; Ghosh, S.; Kim, D.; Chen, H.; Katagiri, A.; Yomogida, Y.; Gao, W.; Yanagi, K.; Kono, J. Groove-Assisted Global Spontaneous Alignment of Carbon Nanotubes in Vacuum Filtration. *Nano Lett.* **2020**, *20* (4), 2332−2338.
(20) Park, S.; Vosguerichian, M.; Bao, Z. A Review of Fabrication and Applications of Carbon Nanotube Film-Based Flexible Electronics. *Nanoscale* **2013**, *5* (5), 1727−1752.
(21) Liu, L.; Han, J.; Xu, L.; Zhou, J.; Zhao, C.; Ding, S.; Shi, H.; Xiao, M.; Ding, L.; Ma, Z.; Jin, C.; Zhang, Z.; Peng, L. M. Aligned, High-Density Semiconducting Carbon Nanotube Arrays for High-Performance Electronics. *Science (80-.).* **2020**, *368* (6493), 850−856.
(22) Gao, W.; Doiron, C. F.; Li, X.; Kono, J.; Naik, G. V. Macroscopically Aligned Carbon Nanotubes as a Refractory Platform for Hyperbolic Thermal Emitters. *ACS Photonics* **2019**, *6* (7), 1602−1609.
(23) Yanagi, K.; Okada, R.; Ichinose, Y.; Yomogida, Y.; Katsutani, F.; Gao, W.; Kono, J. Intersubband Plasmons in the Quantum Limit in Gated and Aligned Carbon Nanotubes. *Nat. Commun.* **2018**, *9*, 1121.
(24) Yamaguchi, S.; Tsunekawa, I.; Komatsu, N.; Gao, W.; Shiga, T.; Kodama, T.; Kono, J.; Shiomi, J. One-Directional Thermal Transport in Densely Aligned Single-Wall Carbon Nanotube Films. *Appl. Phys. Lett.* **2019**, *115*, No. 223104.
(25) Roberts, J. A.; Yu, S. J.; Ho, P. H.; Schoeche, S.; Falk, A. L.; Fan, J. A. Tunable Hyperbolic Metamaterials Based on Self-Assembled Carbon Nanotubes. *Nano Lett.* **2019**, *19* (5), 3131−3137.
(26) Wang, P.; Xiang, R.; Maruyama, S. Thermal Conductivity of Carbon Nanotubes and Assemblies. *Adv. Heat Transfer* **2018**, *50*, 43−122.
(27) Pop, E. Energy Dissipation and Transport in Nanoscale Devices. *Nano Res.* **2010**, *3* (3), 147−169.
(28) Pop, E.; Mann, D. A.; Goodson, K. E.; Dai, H. Electrical and Thermal Transport in Metallic Single-Wall Carbon Nanotubes on Insulating Substrates. *J. Appl. Phys.* **2007**, *101*, No. 093710.
(29) Chen, W. C.; Yin, W. Y.; Jia, L.; Liu, Q. H. Electrothermal Characterization of Single-Walled Carbon Nanotube (SWCNT) Interconnect Arrays. *IEEE Trans. Nanotechnol.* **2009**, *8* (6), 718−728.
(30) Kuroda, M. A.; Cangellaris, A.; Leburton, J. P. Nonlinear Transport and Heat Dissipation in Metallic Carbon Nanotubes. *Phys. Rev. Lett.* **2005**, *95* (26), No. 266803.
(31) Rotkin, S. V.; Perebeinos, V.; Petrov, A. G.; Avouris, P. An Essential Mechanism of Heat Dissipation in Carbon Nanotube Electronics. *Nano Lett.* **2009**, *9* (5), 1850−1855.
(32) Ong, Z.; Pop, E. Molecular Dynamics Simulation of Thermal Boundary Conductance between Carbon Nanotubes and SiO_2. *Phys. Rev. B* **2010**, *81*, No. 155408.
(33) Yu, C.; Shi, L.; Yao, Z.; Li, D.; Majumdar, A. Thermal Conductance and Thermopower of an Individual Single-Wall Carbon Nanotube. *Nano Lett.* **2005**, *5* (9), 1842−1846.
(34) Pop, E.; Mann, D.; Wang, Q.; Goodson, K.; Dai, H. Thermal Conductance of an Individual Single-Wall Carbon Nanotube above Room Temperature. *Nano Lett.* **2006**, *6*, 96−100.
(35) Balandin, A. A. In-Plane and Cross-Plane Thermal Conductivity of Graphene: Applications in Thermal Interface Materials. *Proc. SPIE* **2011**, *8101*, No. 810107.
(36) Nakagawa, K.; Shimura, Y.; Fukazawa, Y.; Nishizaki, R.; Matano, S.; Oya, S.; Maki, H. Microemitter-Based IR Spectroscopy and Imaging with Multilayer Graphene Thermal Emission. *Nano Lett.* **2022**, *22*, 3236−3244.
(37) Alaferdov, A. V.; Savu, R.; Canesqui, M. A.; Vaz, A. R.; Ermakov, V. A.; Moshkalev, S. A.Study of the Thermal Contact between Carbon Nanotubes and a Metal Electrode. *J. Surf. Invest.: X-Ray, Synchrotron Neutron Tech.* **2013**, *7* (4), 607−611.
(38) Dan, B.; Ma, A. W. K.; Hároz, E. H.; Kono, J.; Pasquali, M. Nematic-like Alignment in SWNT Thin Films from Aqueous Colloidal Suspensions. *Ind. Eng. Chem. Res.* **2012**, *51* (30), 10232−10237.
(39) Takahashi, H.; Suzuki, Y.; Yoshida, N.; Nakagawa, K.; Maki, H. High-Speed Electroluminescence from Semiconducting Carbon Nanotube Films. *J. Appl. Phys.* **2020**, *127*, No. 164301.

https://doi.org/10.1021/acs.nanolett.3c02555
Nano Lett. 2023, 23, 9817−9824